Refined line-shape parameters for CO lines broadened by air predicted from requantized classical molecular dynamics simulations

F. Hendaoui, H.T. Nguyen, H. Aroui, N.H. Ngo, H. Tran

Refined line-shape parameters for CO lines broadened by air predicted from requantized classical molecular dynamics simulations

F. Hendaoui[1,2], H. T. Nguyen[3], H. Aroui[2], N. H. Ngo[3,*], H. Tran[1,†]

[1] *Laboratoire de Météorologie Dynamique, IPSL, Sorbonne Université, ENS, Université PSL, École polytechnique, Institut Polytechnique de Paris, CNRS, Paris France*

[2] *Université de Tunis, Laboratoire de Spectroscopie et Dynamique Moléculaire, Ecole Nationale Supérieure d'Ingénieurs de Tunis, 5 Av. Taha Hussein, 1008 Tunis, Tunisia*

[3] *Faculty of Physics, Hanoi National University of Education, 136 Xuan Thuy, Cau Giay, Hanoi, Vietnam*

Abstract

Line-shape parameters and their temperature dependence for CO lines broadened by air have been predicted using requantized classical molecular dynamics simulations. The latter were carried out for mixtures of CO in air for five temperatures ranging from 200 K to 400 K, all at a pressure of 1 atm. For each temperature and pressure condition, various Doppler widths have been considered enabling the calculations of absorption spectra for a large range of collisional to Doppler widths ratios. The simulated spectra were then fitted with the speed-dependent Nelkin-Ghatak, speed-dependent Voigt and Voigt profiles, providing the corresponding line-shape parameters. First-order line-mixing parameters were also retrieved. The temperature dependences of these parameters were then determined using a single power law. Comparisons between the predicted parameters and available experimental values as well as those of the latest edition of the HITRAN database show good agreements. The theoretically predicted values and their temperature dependences can thus be used for the modeling of the absorption spectrum of CO in air and to complete spectroscopic databases when accurate experimentally-determined values are not available.

1. Introduction

Carbon monoxide (CO) is a major air pollutant and a gas trace in the atmosphere, primarily emitted through biomass burning and combustion processes [1]. CO plays an important role in atmospheric chemistry and affects the ability of the atmosphere to cleanse itself of many other polluting gases. Although it does not have a direct effect on the global temperature, model simulations suggest that the observed reduced increase rates of methane may be due to the observed decrease in mean tropospheric CO concentrations and anthropogenic emissions which cause an increase in the global OH concentrations [2]. Reductions in CO are also accompanied by less ozone production in the troposphere, which also reduces global warming. Detailed and continuous observations of carbon monoxide are necessary to better assess their impact on climate and atmospheric pollution. Atmospheric CO concentrations have been measured remotely from space (e.g. [3-8]), ground (e.g. [9]) as well as in local scales (see [10] and references therein). Accurate spectroscopic parameters are needed for the retrieval of atmospheric CO from these in situ and remote sensing measurements. The current version of

* Corresponding author: hoa.nn@hnue.edu.vn
† Corresponding author: ha.tran@lmd.jussieu.fr

the international spectroscopic database HITRAN [11] not only provides the collisional broadening and shifting coefficients but also parameters related to more refined collisional effects such as the speed dependence of the line broadening, the collisional narrowing and line mixing. It was demonstrated in several studies that taking into account these refined line-shape effects can improve atmospheric retrievals (see [12] and references therein). Line-shape parameters are usually obtained from fits of spectra measured in laboratory for given pressure and temperature conditions using a line-shape model. In some recent studies [13-16], we showed that line-shape parameters can be theoretically predicted using requantized classical molecular dynamics simulations (rCMDS). Indeed, using an accurate intermolecular potential, we numerically simulated the time evolution of a system containing a large number of molecules. The auto-correlation function of the dipole moment, responsible for the transition, can thus be computed as well. The Fourier-Laplace transform of this auto-correlation function directly provides the absorption spectrum. Absorption spectra were thereby computed for several molecular systems (e.g. [13-17]). Line-shape parameters were deduced by fitting a line-shape model on the rCMDS-calculated spectra. Comparisons between the predicted line-shape parameters as well as their temperature dependence with those determined from high quality measurements showed very good agreements, even for parameters which have small influences on the spectra [13,14,16]. This method is applied here to predict line-shape parameters for absorption lines of CO broadened by air. The method and data used will be described in the next section of this paper. The analysis of the simulated spectra and the obtained line-shape parameters will be presented in Sec. 3 in which we present the comparisons with data obtained from high resolution measurements as well. The influence of the intermolecular potential on the obtained results will be discussed in the last section together with some conclusions of this work.

2. Requantized classical molecular dynamic simulations and analysis procedure

Molecular dynamics simulations were performed for CO-air mixtures with 50% of CO for a total pressure of 1 atm at 200 K, 250 K, 296 K, 350 K and 400K. The air consists of 21% oxygen (O_2) and 79% nitrogen (N_2) molecules. For each pressure and temperature condition, the calculations were made for about 3×10^8 molecules. This large number of molecules ensures a sufficiently high signal-to-noise ratio of the calculated spectra. At the initial time, these molecules were randomly placed inside cubic boxes with periodic boundary conditions. The initial distance between the molecules was imposed to be larger than 8 Å in order to avoid nonphysical situations associated with too close pairs. Maxwell-Boltzmann distributions were applied to the modulus of the translational and angular velocities of the molecules while random orientations were chosen. The molecular axis orientations were also randomly attributed. The calculations were performed for the equilibrium configuration of the molecules, considered as rigid rotors. Only interactions between CO and N_2 (or O_2) molecules were considered in the simulations. Since the mixtures are at 1 atm and contain 50% of CO, this is equivalent of simulating a system of CO infinitely diluted in air at 0.5 atm. The intermolecular interactions are described by a site-site functional form with two contributions. The first is an electrostatic potential with the sites and charges for CO taken from [18] while those for N_2 and O_2 from [19]. The second term is an atom-atom interaction, expressed by the Lennard-Jones function with parameters determined from those of CO-CO, N_2-N_2 and O_2-O_2 interactions [19] using the Lorentz-Berthelot combination rules [20].

Detailed descriptions of these classical molecular dynamics simulations, which rely on the equations outlined in the chapter 3 of Ref. [21], can be found in [22]. Based on the input intermolecular potential and the initial conditions, the time evolution of the above-mentioned molecular parameters is computed using classical mechanics. Specifically, for each molecule i at time t, we compute the force and torque applied to this molecule (due to its interaction with another one). This enables the determination of the acceleration of its center-of-mass which will be used to change its translational velocity and then to determine the new position of the molecule at time $t + dt$. The angular velocity and the molecular orientation are also incremented from t to $t + dt$. The classical rotation of the CO molecules is requantized using the procedure described in [22], i.e., for a molecule of classical rotational angular momentum ω_i we find the integer J_i for which $\hbar J_i/I$ (with I the moment of inertia) is the closest to ω_i. Once J_i is found, ω_i is requantized by using the new value $\omega_i^{req} = \hbar J_i/I$ while the orientation of the angular momentum is kept unchanged. This requantization corresponds to matching the $P(J_i)$ line positions (note that for simplicity we simulate only the P branch). The normalized auto-correlation function (ACF) of the dipole-moment $\vec{d}_i$(t), carried by the CO molecular axis, was computed for each time step, i.e.:

$$ACF(\omega, t) = \frac{1}{N}\sum_{i=1,N} e^{-i\vec{k}(\omega)[\vec{r}_i(t)-\vec{r}_i(0)]}\,[\vec{d}_i(t)\cdot\vec{d}_i(0)], \quad (1)$$

with $\vec{k}$ the wave vector. The exponential term in Eq. (1) is related to the Doppler effect associated with the translation motion with $\vec{r}_i(t)$ the molecule position and N is the total CO molecule number. The ACFs were computed from $t = 0$ to t_{max}, with $t_{max} = 900$ ps with a time step of 1.8 fs. The latter must be small enough in order to correctly follow the dynamics of the system and should not be too small to save on the computer expense. Note also that due to the imposed minimal distance between the molecules at the initial time, a temporization time, t_{tempo}, was necessary for the system to come to equilibrium and the calculation of the ACF only starts after the thermalization time. t_{tempo} depends on the pressure, temperature, and the minimal distance between the molecules at the initial time. For instance, in the calculations at 296 K considered here, t_{tempo} is 50 ps. The absorption spectrum is directly obtained from the Fourier-Laplace transform of $ACF(\omega, t)$, i.e.:

$$\Phi(\omega) = Re\left\{\frac{1}{\pi}\int_0^\infty ACF(\omega, t)e^{-i\omega t}dt\right\}. \quad (2)$$

In order to simulate the spectra for a wide collisional range (i.e. from the Doppler limit to collision-dominant limit) for an accurate determination of line-shape parameters, the requantized CMDS (rCMDS) were performed with various values of the Doppler width. Indeed, as demonstrated in [13-16], if one neglects the vibrational dependence of the line-shape parameters (which is a very good approximation for all line-shape parameters for CO-air, except the collision-induced line shift), the evolution of the line shapes simulated at a given pressure with various Doppler widths corresponds to that computed for a given Doppler width but with various pressures. Note that since in our rCMDS, we omitted the vibrational dependence of the intermolecular potential, no collision-induced shift can be simulated. In total, 8 Doppler values were used in the calculations which lead to 8 ratios between the collisional width and the Doppler width (e.g. at room temperature $\Gamma_L/\Gamma_D \approx 0.2$, 0.4, 0.6, 1.2, 1.7, 5, 10 and 20).

The simulated spectra were then fitted with different spectral profile models. We chose the most widely-used ones: the Voigt, the quadratic speed dependent Voigt (SDV) [23-25] and the

quadratic speed dependent Nelkin-Ghatak (SDNG) profiles (see [26] and references therein). Collision-induced line-mixing effect was also considered by adjusting the first-order line-mixing parameter [27]. For a given line, the eight simulated spectra were simultaneously fitted in a multi-spectrum fitting procedure, i.e., the line-shape parameters (the collisional line broadening coefficient γ_0 and its speed dependence component γ_2, the Dicke narrowing coefficient β and the first-order line-mixing coefficient ξ) were constrained to be the same for all spectra. For each line, a spectral range of about 3-4 cm^{-1} was considered in the fit, taking into account the influence of neighboring lines. A linear base line was also fitted, individually for each spectrum. Finally, the effect of the limited value of t_{max}, leading to truncated ACFs, was taken into account by convolving the calculated spectrum with a sinus cardinal function of argument $2\pi c\sigma t_{max}$.

The line-shape parameters, corresponding to each used profile, were retrieved for each temperature condition. Then, their temperature dependences were determined using the usual single power law: $A(T) = A(T_0)\left(\frac{T_0}{T}\right)^{n_A}$ with $T_0 = 296$ K, $A(T)$ being either the line broadening coefficient, its speed dependence component, the Dicke narrowing or the line-mixing parameter while n_A is the corresponding temperature exponent. All the obtained parameters and their temperature dependences together with their statistical uncertainty are presented in the next section and reported in Tables 1, 2 and 3.

3. Results and discussions

Examples of absorption spectra calculated with rCMDS are presented in Fig. 1 which also shows the residuals and the root mean square obtained from their fits using the three considered line-shape models, i.e. the Voigt, SDV and SDNG profiles. Note that first-order line-mixing was accounted for only when we used the SDV and the SDNG models. As can be observed in this example, the two more refined profiles lead to much better fit residuals with respect to the Voigt profile. Using the SDNG profile leads to the best residuals, notably better than those obtained with the SDV model showing that Dicke narrowing effect should be taken into account for CO-air.

The line broadening coefficients obtained at 296 K from fit of the rCMDS spectra using the three line-shape models are plotted in Fig. 2. They are compared to data of the spectroscopic database HITRAN [11,28] and to experimental values of Refs. [29] (for the $2 \leftarrow 0$ band) and [30] (for the $1 \leftarrow 0$ band of ^{13}CO, we retain data for ^{13}CO for comparisons, as the line shape parameters for various isotopologues of CO are very similar to each other, see [28] and references therein). Only P branch results are retained for comparison. A good general agreement can be observed. Predicted values of γ_0 obtained with the Voigt profile are weaker than those obtained using the SDV and SDNG profiles, as expected. While the agreement between values of γ_0 obtained with the Voigt profile and those recommended by HITRAN is very satisfactory, our SDV and SDNG values for γ_0 are larger than data associated with the SDV profile of HITRAN. The difference can reach 5.5% for $|m| = 10$. HITRAN data associated with the Voigt profile were obtained by fitting a Padé approximant on the experimental values of γ_0 of [31-33] for various bands while those associated with the SDV were originated from [29,30]. Note that the HITRAN data associated with the SDV are smaller than that associated with the Voigt profile for many lines (Fig. 2). This is in contradiction with the well-known fact that broadening coefficient obtained from fit of a measured or calculated spectrum using the Voigt profile is always smaller than that obtained with a more sophisticated

model such as SDV or SDNG. This is probably due to the accuracy of the different data sets used to deduce HITRAN values and thus calls for more accurate experimental determinations of the air-broadening coefficients of CO. Nevertheless, the uncertainty range for the air-broadening coefficients of CO lines in HITRAN is between 5% and 10% which largely covers the difference between its Voigt and SDV data. Our values predicted from rCMDS without any empirical parameter, are thus in satisfactory agreement with HITRAN data.

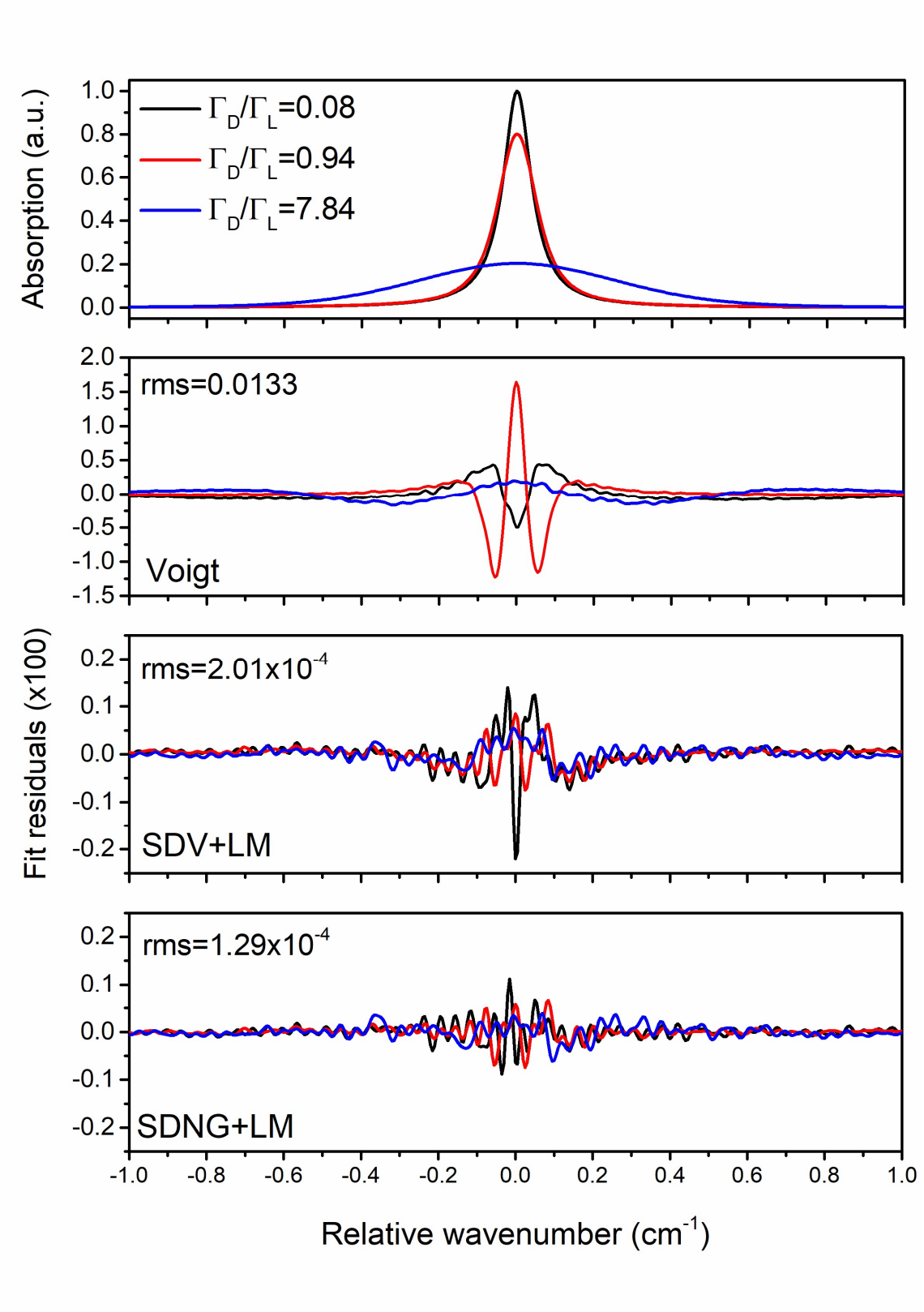

Figure 1: Absorption spectra (top panel) of the P(5) line of CO-air simulated with rCMDS at 200 K and for P_{air} = 0.5 atm and for three Doppler widths. The lower panels show the residuals obtained as the difference between the simulated spectrum and its fit using the Voigt, SDV and SDNG profiles.

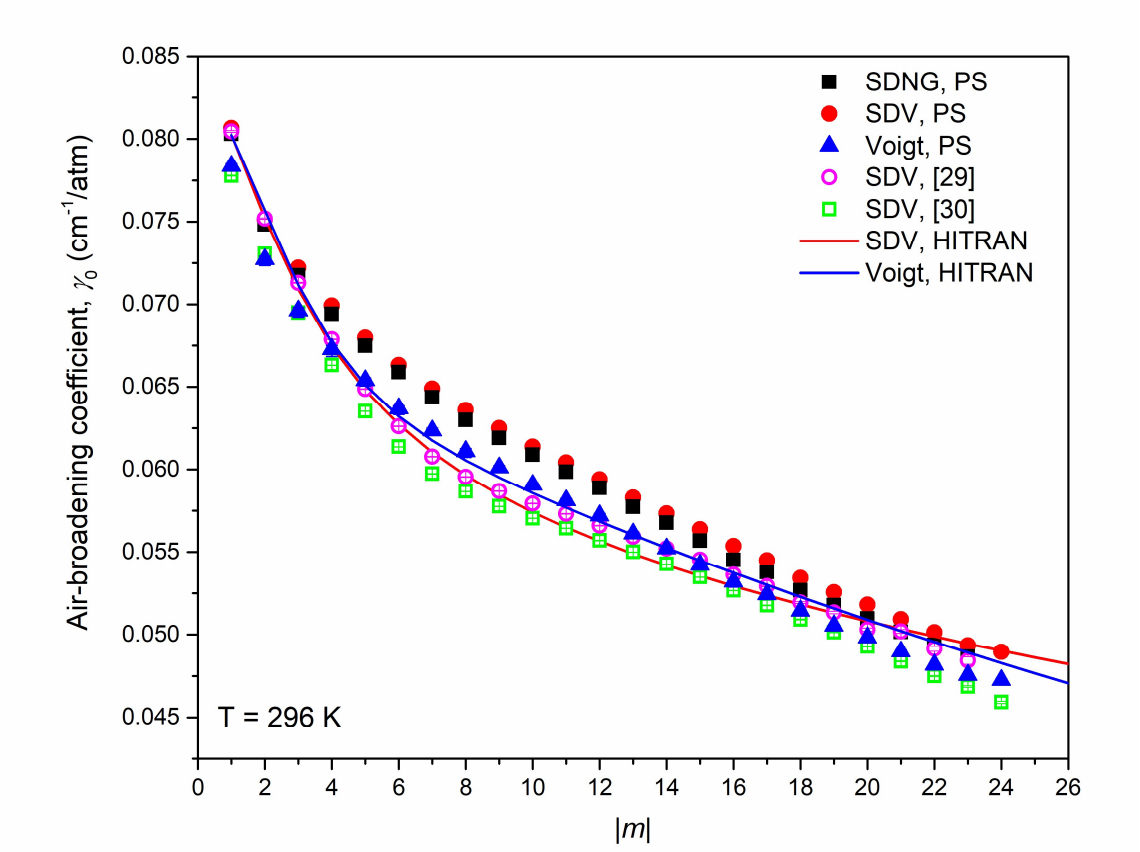

Figure 2: The air-broadening coefficient of CO lines obtained from fits of the rCMDS in the present work (PS) at 296 K with the SDNG, SDV and Voigt profiles and comparison with measured values of [29,30] obtained with the SDV line-shape model. HITRAN data, associated with the Voigt and SDV profiles are also displayed.

Figure 3a displays the values for γ_0 obtained at the five temperatures of the simulations. The adjustment with the SDNG profile was possible only for the most intense lines due to a larger number of adjustable parameters of this model. The values of γ_0 obtained at various temperatures and for each profile were then used to determine the temperature dependence exponent n_{γ_0}. The latter are presented in figure 3b which shows that using the SDNG and SDV profiles to fit the rCMDS spectra lead to very similar values of n_{γ_0}. The difference observed between them for high values of $|m|$ is due to the difficulty to determine γ_0 with the SDNG profile at lower signal to noise ratio. n_{γ_0} obtained with the Voigt profile is larger and is in very good agreement with experimental values of [32] where γ_0 was also obtained with the use of the Voigt profile. However, experimental values of [29,30], associated with the SDV profile are significantly larger than our predictions, with an average difference of about 8%, the maximum difference can reach 12% for $|m| = 14$. Our predictions seem to underestimate the increase of n_{γ_0} starting from $|m| = 5$. Note that only values obtained for P branches of [29,30,32] were retained for comparison since we simulated here the P branch. The relatively small uncertainties, corresponding to the standard deviation of the fit, indicate that a single power law is adequate for the temperature range under consideration. This is further illustrated

in Fig. 4, which exhibits the temperature dependences of γ_0 and γ_2 for the P(3) and P(8) lines, along with their fits using a single power law.

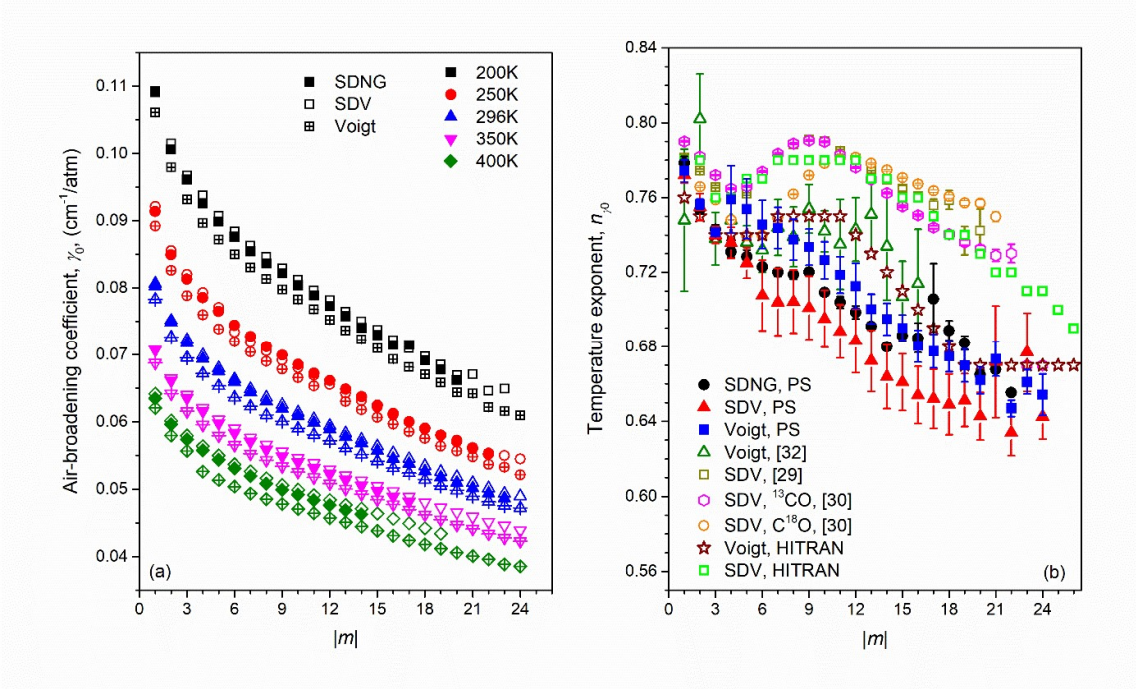

Figure 3: (a) The air-broadening coefficients of CO lines deduced from rCMDS-calculated spectra at various temperatures and with the use of three different line-shape models to fit the simulated spectra. (b) The temperature exponents for air-broadening coefficients deduced from rCMDS spectra and comparison with values in HITRAN2020 [11,28] as well as with the experimental values of [29], [30] and [32].

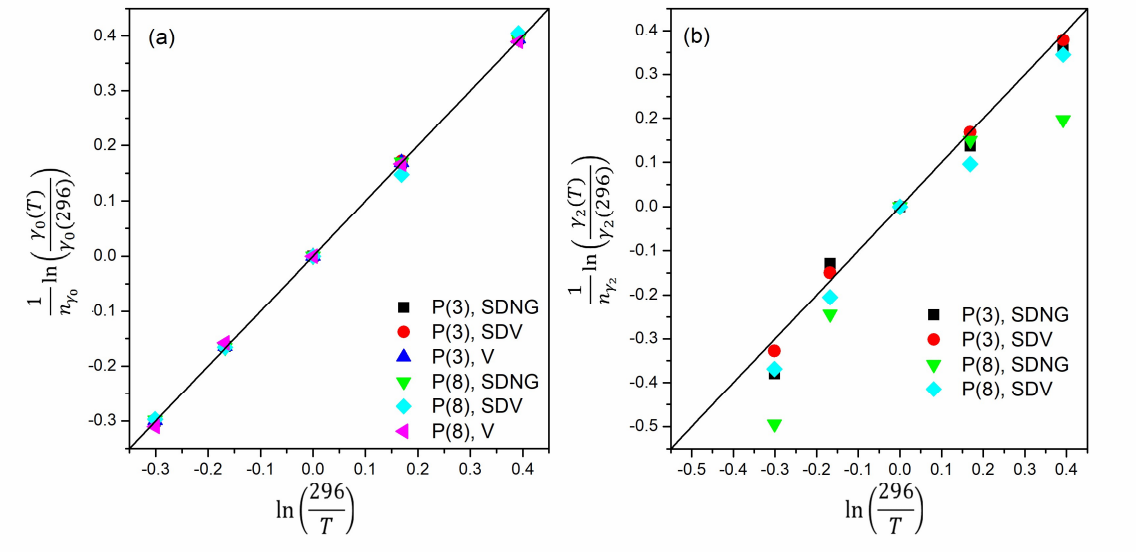

Figure 4: The temperature dependences of γ_0 (a) and γ_2 (b), for the P(3) and P(8) lines, along with their fits using a single power law.

The quadratic speed dependence component of the line broadening, γ_2, were determined from fits of rCMDS spectra with the SDV and SDNG profiles. The obtained values are plotted in Fig. 5a together with data of HITRAN and experimental values of [29,30], both associated with the SDV profile. As can be observed on this figure, our γ_2 values obtained with the SDNG model is lower than those of the SDV profile. This is consistent with previous observations (see [13,14] and references therein) and can be explained by the fact that in general, both Dicke narrowing and speed dependence effects narrow the line. In the SDV profile, the Dicke narrowing effect is neglected, which is compensated by an increase of the retrieved value of γ_2. The experimental values of [29,30] (as well as data in HITRAN, which were obtained by smoothing values of [29,30] using a Paddé approximant), associated with the SDV profile are in rather good agreement with our SDNG values but not with those obtained using the SDV model. The temperature dependence exponent of γ_2 is displayed in Fig. 5b. We observe that n_{γ_2} obtained with the rCMDS spectra is smaller than n_{γ_0} (Fig. 3b). This is consistent with rCMDS-predicted results but also with experimental determinations for N_2-broadened CO_2 lines [13,34]. Note that in the HITRAN database as in many studies, n_{γ_2} is assumed to be the same as n_{γ_0}.

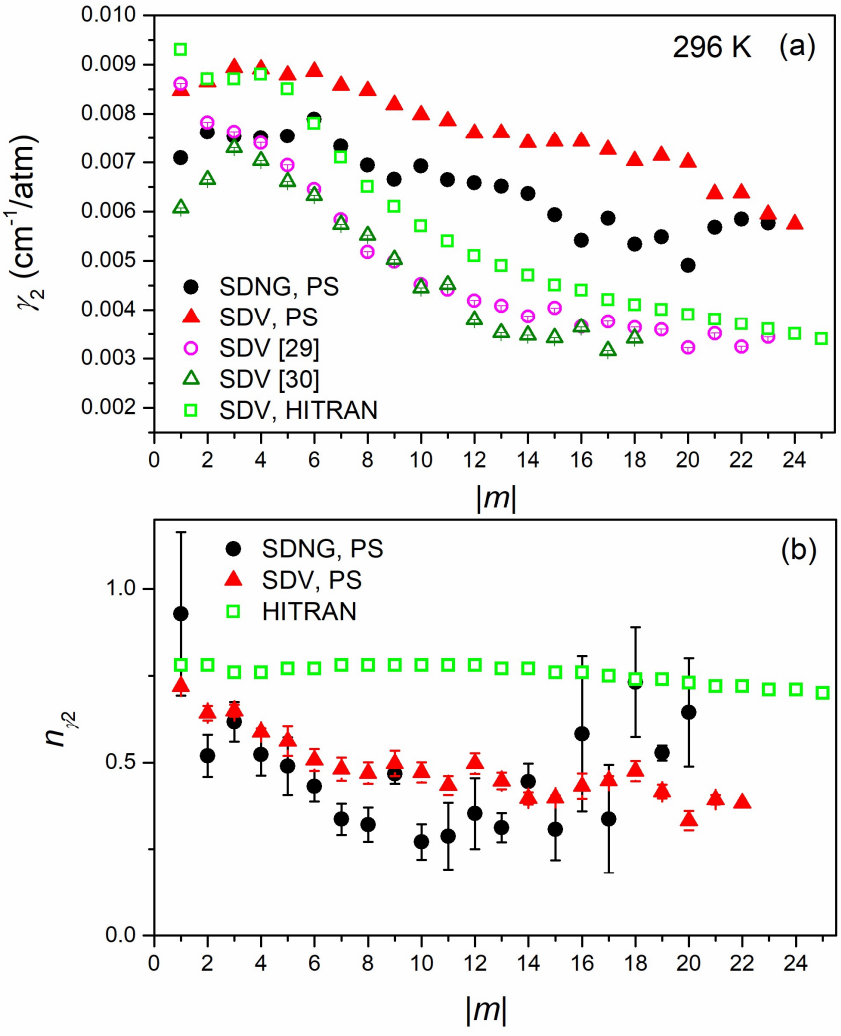

Figure 5: (a): The quadratic speed dependence component of the line broadening obtained from rCMDS at 296 K and its comparison with HITRAN data as well as measured values of [29] and [30]. (b) The temperature dependence of γ_2, n_{γ_2}, obtained from rCMDS spectra with the use of the SDV and SDNG profiles. Values in HITRAN, assumed to be the same as for n_{γ_0} are also displayed.

The Dicke narrowing parameter, β deduced from fits of the rCMDS spectra with the SDNG model at room temperature is presented in the top panel of Fig. 6. It is well known that this coefficient strongly depends on the line-shape model used to fit the measured/simulated spectra. For the same line, values obtained with the SDNG or the Nelkin–Ghatak (without speed dependence) model can be completely different. To the best of our knowledge, there is no available data for β obtained with the SDNG profile for air-broadened CO lines. The predicted values of β are on the same order of magnitude as those of γ_2 which shows that Dicke narrowing effect plays a role for CO-air, which is confirmed by the results shown in Fig. 1 where fit residuals obtained with the SDNG model is notably improved with respect to the SDV profile. The deduced temperature dependence of the Dicke narrowing parameter, n_β, is displayed in the bottom panel of Fig. 6. n_β is quite close to unity and associated with large error bars. We thus suggest to use $n_\beta = 1$ for all lines.

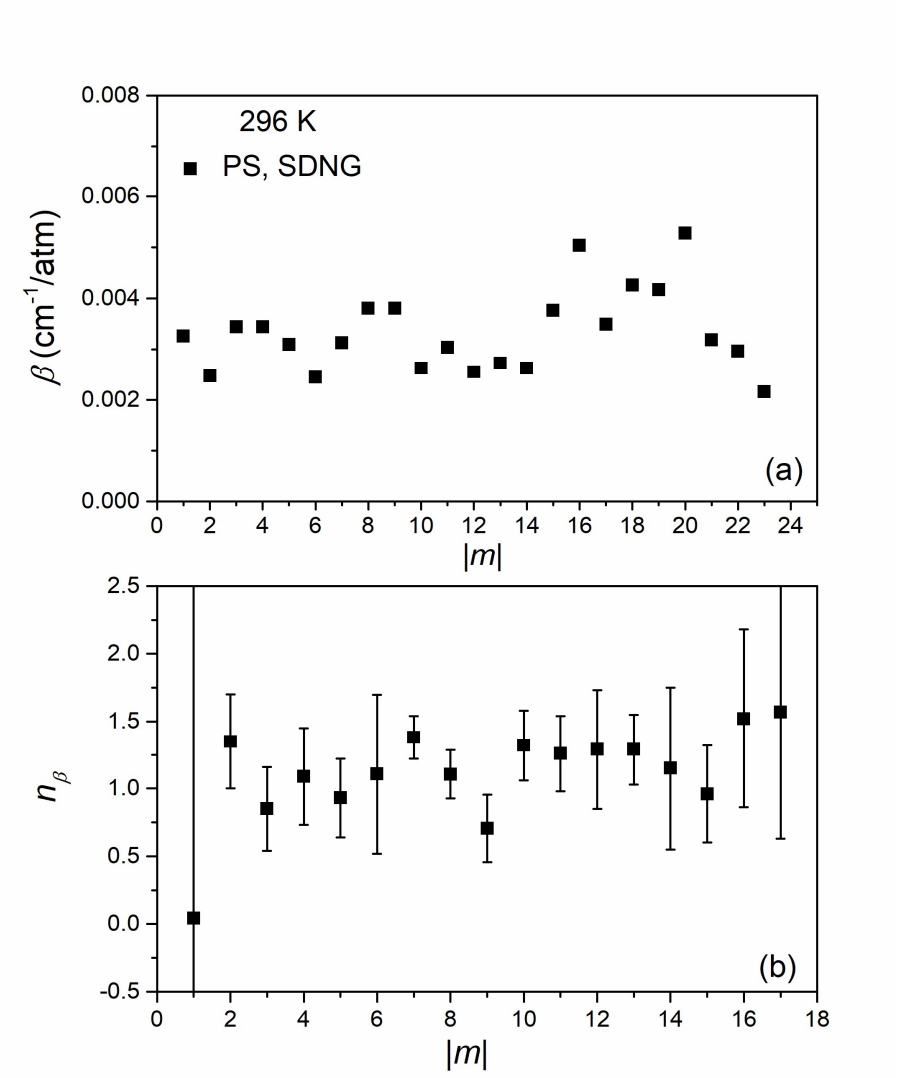

Figure 6: The Dicke narrowing parameter at 296 K (a) and its temperature dependence exponent (b), obtained from fits of the rCMDS spectra with the SDNG profile.

Figure 7a presents the rCMDS predicted first-order line- mixing parameters, ζ at 296 K. The predicted values are compared with measured values of [29] for the 2 ← 0 band, obtained with the SDV profile. They are also compared with those computed using an Exponential Power Gap scaling law [28] which are used in the HITRAN database. Firstly, we can observe that the line-mixing parameter only slightly depends on the used line-shape model, as previously observed for CO_2 [14]. Secondly, our parameters are in very good agreement with experimental data of [29] and modeled values of [28]. The temperature dependence of the rCMDS-predicted ζ is presented in Fig. 7b, the plotted error bar being the uncertainties due to the fit of the temperature exponents. As can be observed, the uncertainty is large showing that the single power law may not be the most adapted function to model the temperature dependence of the line-mixing parameter. Considering the large uncertainty of n_ζ and its random variation with m, we suggest to use the constant and averaged value of 1.2 for n_ζ with both the SDV and SDNG profiles.

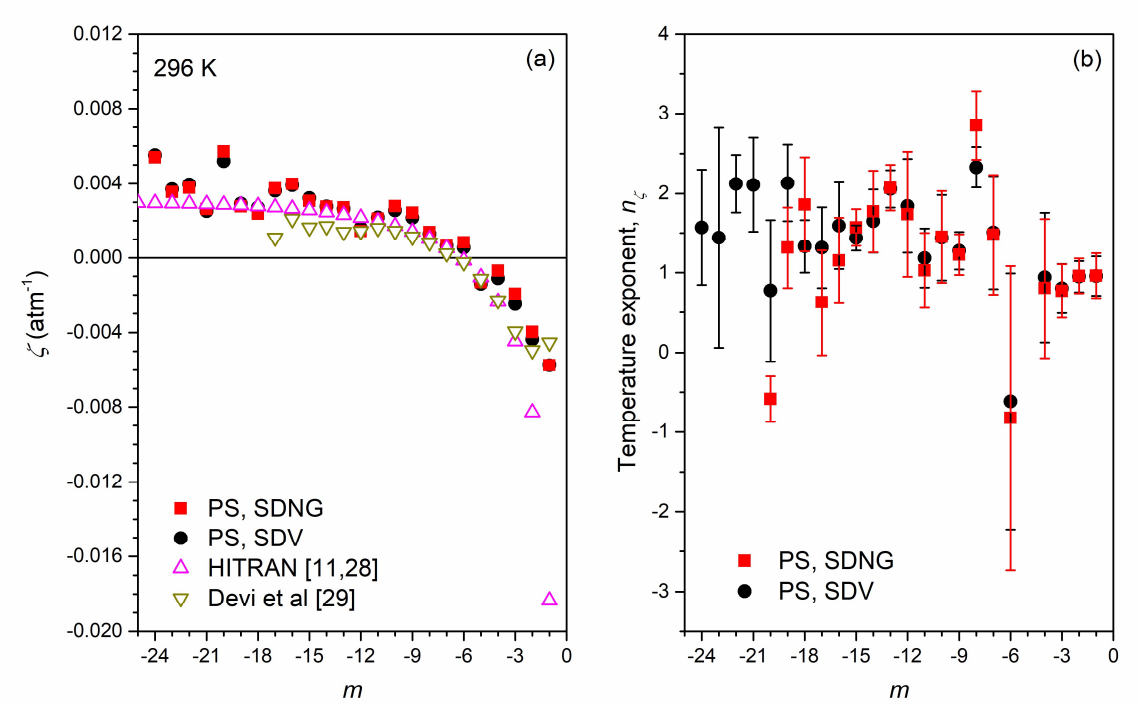

Fig. 7: (a) The first-order line-mixing parameter obtained in this work by fitting the rCMDS spectra with the SDV and SDNG profiles and comparison with experimentally-determined values of [29] as well as HITRAN data. (b) The temperature dependence of ζ.

4. Conclusion

Line-shape parameters for air-broadened CO lines (J up to 24) corresponding to the Voigt, the quadratic speed-dependent Voigt and the quadratic speed-dependent Nelkin-Ghatak profiles have been predicted using requantized classical molecular dynamics simulations (rCMDS). The latter have been performed for temperature ranging from 200K to 400 K enabling to determine the temperature dependence of various line-shape parameters. Comparisons with available data show good agreement for the air-broadening and line-mixing coefficients while larger differences are obtained for the speed dependence of the line broadening. In particular, we show that taking into account the Dicke narrowing effect through the use of the SDNG profile appreciably reduces the fit residuals and that the predicted temperature dependence of the speed dependent parameter is well smaller than that of the broadening coefficient. The predicted line-shape parameters and their temperature dependence can be used for the modeling of the absorption spectrum of CO in air and to complete spectroscopic databases when accurate experimentally-determined values are not available. The present work again validates the use of the rCMDS method to describe collisional effects on the spectral profile and to predict line-shape parameters and their temperature dependence. Note that the obtained results depend on the quality and the precision of the used intermolecular potential. In the present study, tests have been made with different electrostatic contributions of the potential, i.e. those of Refs. [18], [19] and [35]. The obtained results show that the values of the charges for CO taken from [18] lead to predicted line broadening coefficients which are in good agreement with measured values while those predicted with the charges taken from [19] and [35] overestimate the half-widths by more than 12%. Further investigations on the influence of the used potential energy

surface on the calculated spectra and the deduced line-shape parameters will be conducted in a forthcoming study.

Line	γ_0^V(296 K)	n_{γ_0}
P(1)	0.0784(1)	0.774 (6)
P(2)	0.0727(1)	0.757 (3)
P(3)	0.0696(1)	0.742 (2)
P(4)	0.0673(1)	0.759 (18)
P(5)	0.0654(1)	0.754 (16)
P(6)	0.0637(1)	0.746 (13)
P(7)	0.0624(1)	0.744 (11)
P(8)	0.0611(1)	0.738 (11)
P(9)	0.0601(1)	0.734 (10)
P(10)	0.0591(1)	0.726 (10)
P(11)	0.0581(1)	0.719 (10)
P(12)	0.0572(1)	0.713 (12)
P(13)	0.0561(1)	0.700 (8)
P(14)	0.0552(1)	0.695 (9)
P(15)	0.0542(1)	0.690 (7)
P(16)	0.0532(1)	0.680 (9)
P(17)	0.0524(1)	0.678 (9)
P(18)	0.0514(1)	0.675 (8)
P(19)	0.0505(1)	0.670 (9)
P(20)	0.0498(1)	0.662 (7)
P(21)	0.0490(1)	0.673 (9)
P(22)	0.0482(1)	0.647 (5)
P(23)	0.0476(1)	0.661 (7)
P(24)	0.0472(1)	0.654 (11)

Table 1: Line broadening coefficients for air-broadened CO lines, deduced from fits of rCMDS spectra with the Voigt profile, at 296 K, γ_0^V(296 K) (cm^{-1}/atm) and their temperature dependence exponents n_{γ_0}.

Line	γ_0^{SDV}(296 K)	n_{γ_0}	γ_2^{SDV}(296 K)	n_{γ_2}	ξ^{SDV}(296 K)
P(1)	0.0807(1)	0.772 (5)	0.0085(1)	0.720 (4)	-0.0057(2)
P(2)	0.0751(1)	0.755 (7)	0.0087(1)	0.642 (3)	-0.0044(2)
P(3)	0.0722(1)	0.740 (5)	0.0089(1)	0.649 (17)	-0.0025(2)
P(4)	0.0699(1)	0.736 (9)	0.0089(1)	0.588 (11)	-0.0011(1)
P(5)	0.0680(1)	0.725 (8)	0.0088(1)	0.562 (43)	-0.0014(1)
P(6)	0.0663(1)	0.708 (19)	0.0089(1)	0.507 (32)	0.0005(1)
P(7)	0.0649(1)	0.704 (18)	0.0086(1)	0.481 (33)	0.0006(1)
P(8)	0.0636(1)	0.704 (17)	0.0085(1)	0.469(31)	0.0013(2)
P(9)	0.0625(1)	0.701 (17)	0.0082(1)	0.498 (36)	0.0022(2)
P(10)	0.0614(1)	0.695 (16)	0.0080(1)	0.472 (29)	0.0026(2)
P(11)	0.0604(1)	0.688 (15)	0.0079(1)	0.434 (27)	0.0022(2)
P(12)	0.0594(1)	0.683 (17)	0.0076(1)	0.497 (30)	0.0016(2)
P(13)	0.0583(1)	0.672 (17)	0.0076(1)	0.447 (24)	0.0026(2)
P(14)	0.0573(1)	0.664 (17)	0.0074(1)	0.397 (18)	0.0028(2)
P(15)	0.0564(1)	0.661 (15)	0.0074(1)	0.398 (7)	0.0032(2)
P(16)	0.0554(1)	0.654 (16)	0.0074(1)	0.432 (36)	0.0039(3)
P(17)	0.0545(1)	0.652 (16)	0.0073(1)	0.448 (14)	0.0036(3)
P(18)	0.0534(1)	0.649 (16)	0.0070(1)	0.475 (13)	0.0027(4)

P(19)	0.0526(1)	0.651 (14)	0.0071(1)	0.416 (29)	0.0029(5)
P(20)	0.0518(1)	0.643 (13)	0.0070(1)	0.333 (20)	0.0052(6)
P(21)	0.0509(1)	0.672 (30)	0.0064(1)	0.393 (28)	0.0025(8)
P(22)	0.0501(1)	0.634 (12)	0.0064(2)	0.383 (14)	0.0040(12)
P(23)	0.0494(1)	0.677 (21)	0.0059(1)		0.0037(6)
P(24)	0.0490(1)	0.643 (12)	0.0057(1)		0.0055(3)

Table 2: Line-shape parameters for air-broadened CO lines, deduced from fits of rCMDS spectra with the speed dependent Voigt profile and their temperature dependence. γ_0^{SDV}(296 K), γ_2^{SDV}(296 K) and ξ^{SDV}(296 K) are the broadening coefficient (cm^{-1}/atm), the speed dependent parameter (cm^{-1}/atm) and the first-order line-mixing parameter (atm^{-1}) while n_{γ_0} and n_{γ_2} are the temperature dependence exponents of γ_0^{SDV} and γ_2^{SDV}, respectively.

Line	γ_0^{SDNG}(296K)	n_{γ_0}	γ_2^{SDNG}(296 K)	n_{γ_2}	β^{SDNG}(296 K)	ξ^{SDNG}(296 K)
P(1)	0.0803(1)	0.779 (4)	0.0071(1)	0.928 (235)	0.0033(2)	-0.0057(2)
P(2)	0.0748(1)	0.754 (3)	0.0076(1)	0.519 (60)	0.0025(1)	-0.0040(2)
P(3)	0.0717(1)	0.743 (3)	0.0075(1)	0.616 (57)	0.0035(1)	-0.0020(1)
P(4)	0.0694(1)	0.731 (3)	0.0075(1)	0.523 (60)	0.0034(1)	-0.0007(1)
P(5)	0.0675(1)	0.728 (4)	0.0075(1)	0.489 (83)	0.0031(1)	-0.0013(1)
P(6)	0.0659(1)	0.723 (2)	0.0079(1)	0.432 (45)	0.0024(1)	0.0008(1)
P(7)	0.0644(1)	0.720 (3)	0.0073(1)	0.337 (45)	0.0031(1)	0.0007(1)
P(8)	0.0630(1)	0.719 (3)	0.0069(1)	0.321 (50)	0.0038(1)	0.0014(1)
P(9)	0.0619(1)	0.720 (2)	0.0067(1)	0.467 (29)	0.0038(1)	0.0024(1)
P(10)	0.0609(1)	0.709 (2)	0.0069(1)	0.271 (51)	0.0026(1)	0.0028(2)
P(11)	0.0599(1)	0.704 (4)	0.0066(1)	0.288 (97)	0.0030(1)	0.0021(2)
P(12)	0.0589(1)	0.699 (4)	0.0066(1)	0.353 (102)	0.0026(1)	0.0014(2)
P(13)	0.0577(1)	0.691 (2)	0.0065(1)	0.312 (42)	0.0027(1)	0.0027(2)
P(14)	0.0568(1)	0.680 (3)	0.0064(1)	0.445 (52)	0.0026(1)	0.0028(2)
P(15)	0.0557(1)	0.686 (3)	0.0059(1)	0.307 (89)	0.0038(1)	0.0031(2)
P(16)	0.0545(1)	0.685 (8)	0.0054(1)	0.583 (224)	0.0050(1)	0.0040(3)
P(17)	0.0538(1)	0.706 (19)	0.0059(1)	0.337 (156)	0.0035(2)	0.0038(3)
P(18)	0.0527(1)	0.689 (6)	0.0053(1)	0.731 (158)	0.0043(2)	0.0024(4)
P(19)	0.0518(1)	0.682 (4)	0.0055(1)	0.528 (22)	0.0042(2)	0.0028(5)
P(20)	0.0510(1)	0.665 (2)	0.0049(1)	0.645 (156)	0.0053(2)	0.0057(6)
P(21)	0.0502(1)	0.668	0.0057(2)		0.0032(2)	0.0026(8)
P(22)	0.0494(1)	0.655	0.0058(2)		0.0030(2)	0.0038(11)
P(23)	0.0487(1)		0.0058(1)		0.0022(2)	0.0035(3)

Table 3: Line-shape parameters for air-broadened CO lines, deduced from fits of rCMDS spectra with the speed dependent Nelkin-Ghatak profile and their temperature dependence. γ_0^{SDNG}(296 K), γ_2^{SDNG}(296 K), β^{SDNG}(296 K) and ξ^{SDNG}(296 K) are the broadening coefficient (cm^{-1}/atm), the speed dependent (cm^{-1}/atm), the Dicke narrowing parameter (cm^{-1}/atm) and the first-order line-mixing parameter (atm^{-1}) while n_{γ_0} and n_{γ_2} are the temperature dependence exponents of γ_0^{SDNG} and γ_2^{SDNG}, respectively.

References

[1] Duncan BN, Logan JA, Bey I, Megretskaia IA, Yantosca RM, Novelli PC, et al. Global budget of CO, 1988–1997: source estimates and validation with a global model. J Geophys Res 2007;112(D22). doi:10.1029/2007JD008459.

[2] Bruhl Ch, Crutzen PJ. Reductions in the anthropogenic emissions of CO and their effect on CH_4. Chemosphere: Global Change Science 1999;1:249-254.

[3] McMillan WW, Barnet C, Strow L, Chahine MT, McCourt ML, Warner JX, Novelli PC, Korontzi S, Maddy ES, Datta S. Daily global maps of carbon monoxide from NASA's Atmospheric Infrared Sounder. Geophys Res Let, 2005 https://doi.org/10.1029/2004GL021821

[4] Clerbaux C, Boynard A, Clarisse L, George M, Hadji-Lazaro J, Herbin H, Hurtmans D, Pommier M, Razavi A, Turquety S, Wespes C, Coheur PF. Monitoring of atmospheric composition using the thermal infrared IASI/MetOp sounder. Atmos Chem Phys 2009;9:6041–6054. https://doi.org/10.5194/acp-9-6041-2009

[5] Drummond JR, Zou J, Nichitiu F, Kar J, Deschambaut R, Hackett J. A review of 9-year performance and operation of the MOPITT instrument. Adv Space Res 2010;45:760–774. https://doi.org/10.1016/j.asr.2009.11.019

[6] de Laat ATJ, Gloudemans AMS, Aben I, Schrijver H. Global evaluation of SCIAMACHY and MOPITT carbon monoxide column differences for 2004–2005. J Geophys Res 2010;115:D06307. https://doi.org/10.1029/2009JD012698

[7] Luo M, Shephard MW, Cady-Pereira KE, Henze DK, Zhu L, Bash JO, Pinder RW, Capps SL, Walker JT, Jones MR. Satellite observations of tropospheric ammonia and carbon monoxide: Global distributions, regional correlations and comparisons to model simulations. Atmos Env 2015;106:262-277.

[8] Schneising O, Buchwitz M, Reuter M, Bovensmann H, Burrows JP, Borsdorff T, Deutscher NM, Feist DG, Griffith DWT, Hase F, Hermans C, Iraci LT, Kivi R, Landgraf J, Morino I, Notholt J, Petri C, Pollard DF, Roche S, Shiomi K, Strong K, Sussmann R, Velazco VA, Warneke T, Wunch D. A scientific algorithm to simultaneously retrieve carbon monoxide and methane from TROPOMI onboard Sentinel-5 Precursor. Atmos Meas Tech 2019;12:6771–6802. https://doi.org/10.5194/amt-12-6771-2019.

[9] Sha MK, Langerock B, Blavier JFL, Blumenstock T, et al. Validation of methane and carbon monoxide from Sentinel-5 Precursor using TCCON and NDACC-IRWG stations. Atmos Meas Tech 2021;14:6249–6304. https://doi.org/10.5194/amt-14-6249-2021

[10] Zellweger C, Steinbrecher R, Laurent O, Lee H, Kim S, Emmenegger L, Steinbacher M, Buchmann B. Recent advances in measurement techniques for atmospheric carbon monoxide and nitrous oxide observations. Atmos Meas Tech 2019;12:5863–5878. https://doi.org/10.5194/amt-12-5863-2019

[11] Gordon IE, Rothman LS, Hargreaves RJ, Hashemi R, Karlovets EV, Skinner FM, Conway EK, Hill C, Kochanov RV, Tan Y, Wcisło P, Finenko AA, Nelson K, Bernath PF, Birk M et al.. The HITRAN2020 molecular spectroscopic database. J Quant Spectrosc Radiat Transf, 277, 2022, 107949. https://doi.org/10.1016/j.jqsrt.2021.107949

[12] Hartmann JM, Tran H, Armante R, Boulet C, Campargue A, Forget F, Gianfrani L, Gordon IE, Guerlet S, Gustafsson M, Hodges JT, Kassi S, Lisak D, Thibault F, Toon GC. Recent advances in collisional effects on spectra of molecular gases and their practical consequences. J Quant Spectrosc Radiat Transf 2018;213:178-227.

[13] Nguyen HT, Ngo NH, Tran H. Prediction of line shape parameters and their temperature dependences for CO_2–N_2 using molecular dynamics simulations. J Chem Phys 2018;149:224301. https://doi.org/10.1063/1.5063892

[14] Nguyen HT, Ngo NH, Tran H. Line-shape parameters and their temperature dependences predicted from molecular dynamics simulations for O_2- and air-broadened CO_2 lines. J Quant Spectrosc Radiat Transf 2020;242:106729.

[15] Tran DD, Sironneau VT, Hodges JT, Armante R, Cuesta J, Tran H. Prediction of high-order line-shape parameters for air-broadened O_2 lines using requantized classical molecular dynamics

simulations and comparison with measurements. J Quant Spectrosc Radiat Transf 2019;222-223: 108-114.

[16] Ngo NH, Nguyen HT, Le MT, Tran H. Air-broadened N_2O line-shape parameters and their temperature dependences by requantized classical molecular dynamics simulations. J Quant Spectrosc Radiat Transf 2021;267:107607.

[17] Ngo NH, Le MT, Tran H, Hartmann JM. Molecular dynamics simulations of pressure-broadened symmetric-top gas spectra. Application to CH_3F-Ar and CH_3F-He mixtures. J Quant Spectrosc Radiat Transf 2022;278:108031.

[18] Karssemeijer LJ, Ioppolo S, van Hemert MC, van der Avoird A, Allodi MA, Blake GA, Cuppen HM. Dynamics of CO in amorphous water-ice environments. The Astrophysical Journal 2014;781:16. https://doi:10.1088/0004-637X/781/1/16

[19] Bouanich P. Site-site Lennard-Jones potential parameters for N_2, O_2, H_2, CO and CO_2. J Quant Spectrosc Radiat Transf 1992;47:243-50.

[20] Hirschfelder JE, Curtiss CF, Bird RB. Molecular theory of gases and liquids, Wiley, New York, 1954

[21] Allen MP, Tildesley DJ. Computer simulations of liquids. Oxford: Oxford Uni- 429 versity Press; 1987.

[22] Hartmann JM, Tran H, Ngo NH, Landsheere X, Chelin P, Lu Y, Liu AW, Hu SM, Gianfrani L, Casa G, Castrillo A, Lepère M, Delière Q, Dhyne M, Fissiaux L. *Ab ini t io* calculations of the spectral shapes of CO2 isolated lines including non-Voigt effects and comparisons with experiments. Phys Rev A 2013;87:013403.

[23] Berman PR. Speed-dependent collisional width and shift parameters in spectral profiles. J Quant Spectrosc Radiat Transf 1972; 12: 1331–42.

[24] Rohart F, Mader H, Nicolaisen H-W. Speed dependence of rotational relaxation induced by foreign gas collisions: studies on CH_3F by millimeter wave coherent transients. J Chem Phys 1994; 101: 6475–86.

[25] Rohart F, Ellendt A, Kaghat F, Mäder H. Self and polar foreign gas line broadening and frequency shifting of CH_3F: effect of the speed dependence observed by millimeter-wave coherent transients. J Mol Spectrosc 1997; 185:222–33.

[26] Ngo NH, Lisak D, Tran H, Hartmann JM. An isolated line-shape model to go beyond the Voigt profile in spectroscopic databases and radiative transfer codes. J Quant Spectrosc Radiat Transf 2013;129:89-100.

[27] Rosenkranz PW. Shape of the 5 mm oxygene band in the atmosphere. IEEE Trans. Antennas Propag 1975;AP-23:498-506.

[28] Hashemi R, Gordon IE, Adkins EM, Hodges JT, Long DA, Birk M, Loos J, Boone CD, Fleisher AJ, Predoi-Cross A, Rothman LS. Intensities, collision-broadened half-widths, and collision-induced line shifts in the second overtone band of $^{12}C^{16}O$. J Quant Spectrosc Radiat Transf 2021;271: 107735.

[29] Devi MV, Benner CD, Smith MAH, Mantz AW, Sung K, Brown LR, Predoi-Cross A. Spectral line parameters including temperature dependences of self- and air-broadening in the 2-0 band of CO at 2.3 μm. J Quant Spectrosc Radiat Transf 2012;113:1013–1033.

[30] Devi MV, Benner CD, Sung K, Crawford TJ, Li G, Gamache RR, Smith MAH, Gordon IE, Mantz AW. Positions, intensities and line shape parameters for the $1 \leftarrow 0$ bands of CO isotopologues. J Quant Spectrosc Radiat Transf 2018;218:203–230.

[31] Régalia-Jarlot L, Thomas X, Von der Heyden P, Barbe A. Pressure-broadened line widths and pressure-induced line shifts coefficients of the (1-0) and (2-0) bands of $^{12}C^{16}O$. J Quant Spectrosc Radiat Transf 2005;91:121-131.

[32] Zou Q, Varanasi P. New laboratory data on the spectral line parameters in the 1-0 and 2-0 bands of $^{12}C^{16}O$ relevant to atmospheric remote sensing. J Quant Spectrosc Radiat Transf 2002:75:63-92.

[33] Sung K, Varanasi P. Intensities, collision-broadened half-widths, and collision-induced line shifts in the second overtone band of $^{12}C^{16}O$. J Quant Spectrosc Radiat Transf 2004;83:445-458.

[34] Wilzewski JS, Birk M, Loos J, Wagner G. Temperature-Dependence Laws of Absorption Line Shape Parameters of the CO_2 ν_3 Band. J Quant Spectrosc Radiat Transf 2018;206:296-305.

[35] Chetty N, Coulinga VW. Measurement of the electric quadrupole moment of CO. J Chem Phys 2011;134:164307. https://doi.org/10.1063/1.3585605